

---

## Failure precursor detection in complex electrical systems using symbolic dynamics

---

R.P. Patankar\*

Intelligent Automation, Inc.,  
Rockville, MD 20855, USA  
Fax: 301-294-5248  
E-mail: rpatankar@i-a-i.com    E-mail: rppatank@mtu.edu  
\*Corresponding author

V. Rajagopalan

Electrical Engineering,  
Pennsylvania State University,  
University Park, PA 16802, USA  
E-mail: vxr139@psu.edu

A. Ray

Mechanical Engineering,  
Pennsylvania State University,  
University Park, PA 16802, USA  
E-mail: axr2@psu.edu  
Website: <http://www.mne.psu.edu/Ray/>

**Abstract:** Failures in a plant's electrical components are a major source of performance degradation and plant unavailability. In order to detect and monitor failure precursors and anomalies early in electrical systems, we have developed a signal processing method that can detect and map patterns to an anomaly measure. Application of this technique for failure precursor detection in electronic circuits resulted in robust detection. This technique was observed to be superior to conventional pattern recognition techniques such as neural networks and principal component analysis for anomaly detection. Moreover, this technique based on symbolic dynamics offers superior robustness due to averaging associated with experimental probability calculations. It also provided a monotonically increasing smooth anomaly plot which was experimentally repeatable to a remarkable accuracy.

**Keywords:** symbolic dynamics; anomaly detection; health monitoring.

**Reference** to this paper should be made as follows: Patankar, R.P., Rajagopalan, V. and Ray, A. (2008) 'Failure precursor detection in complex electrical systems using symbolic dynamics', *Int. J. Signal and Imaging Systems Engineering*, Vol. 1, No. 1, pp.68-77.

**Biographical notes:** Ravindra Patankar graduated from the Indian Institute of Technology, Bombay with a five-year integrated Master of Technology Degree in Mechanical Engineering in 1994. In 1999, he earned a PhD in Mechanical Engineering from The Pennsylvania State University. He was a Project Engineer at Delphi Corporation's Steering Headquarters in Saginaw, Michigan from 1999 to 2001. From 2001 to 2004, he was an Assistant Professor of Mechanical Engineering-Engineering Mechanics at Michigan Technological University. From 2004 to 2007, he was a Program Manager at Intelligent Automation, Inc. of Rockville. He has recently accepted a Principal Systems Engineer position at Honeywell Aerospace.

Venkatesh Rajagopalan obtained his Bachelor's Degree in Electrical Engineering from the University of Madras in 2001. He received the MS and PhD Degrees in Electrical Engineering from the Pennsylvania State University in 2003 and 2007, respectively. His general research interests include fault detection, signal processing and control systems. He is a member of the Institute of Electrical and Electronics Engineers (IEEE). He was a research engineer in Mathworks, Inc. until December 2007. Currently, he is on the research staff of General electric Company at Bangalore, India.

Asok Ray earned the PhD Degree in Mechanical Engineering from Northeastern University and also Graduate Degrees in Electrical Engineering, Computer Science, and Mathematics. He joined the Pennsylvania State University in July 1985, and is currently a Distinguished Professor of

Mechanical Engineering, and a Graduate Faculty of Electrical Engineering. He has authored or co-authored over 400 research publications, including about 200 scholarly papers in refereed journals and research monographs. He is a Fellow of IEEE, a Fellow of ASME, and a Fellow of World Innovation Foundation (WIF).

## 1 Introduction

Sensing and estimation of failure precursors are critical for operation and control of complex electrical systems; e.g., aerospace, electric power generation, nuclear reactors. Here, complex systems are non-linear systems with possibility of chaos. Dependability of complex systems is achieved by identifying and mitigating the origins of chaos and disorder at a very early stage through dynamic coordination and control of the critical subsystems. Failures in a plant's electrical components are a major source of performance degradation and plant unavailability. Therefore, for real-time control and operation, it is necessary to develop the capability of sensing failure precursors. Installing failure sensors at specific sites is expensive. Moreover, there are cases where direct measurements at an early stage are not possible due to the lack of appropriate sensing hardware.

Early detection of failure precursors in a complex system requires knowledge of its dynamical behaviour, which is derived either from physics-based models or time series data or both. Since accurate and computationally tractable modelling of complex system dynamics is often infeasible solely based on the fundamental principles of physics, it is necessary to rely on time series data from sensors and other sources of information. Along this line, Ray (2004) reported a new concept of anomaly detection in complex dynamical systems via Symbolic Time Series Analysis (STSA). This concept is the basis for the development of a computer-integrated failure precursor/anomaly sensing system based on available input/output information. The structure of this precursor sensing system has the capability to combine the inputs from a network of several distributed systems.

The structures of failure estimator models have been predominantly static or linear dynamic. Anomaly monitoring algorithms, based on these models, are computationally simple and easy to implement. Although these algorithms are capable of diagnosing faults that have already occurred, they are unsuitable for early detection of failure precursors which follow non-linear dynamics. Hence they are often inadequate for prognosis in practical applications. This problem could be alleviated by extracting the hidden information from the data, especially in the early failure precursor regime. From this perspective, the roles of physics-based modelling and signal processing of non-linear time series data have become significantly more critical due to the need to capture the complex dynamics.

In most systems, failures, even if they appear to be sudden, are a result of a slowly growing, non-stationary

anomaly. In contrast, the mundane system dynamics is very fast. This physical fact about anomalies is ignored by the conventional anomaly detection algorithms; but we have exploited this fact. From this perspective, anomaly detection via *symbolic dynamics* (Lind and Marcus, 1995) and information theory (Cover and Thomas, 1991) was ideally suited to filter out the dominant part of the response, due to fast dynamics, from the small-signal deviations in the data due to anomaly evolution in its early stages. Maps of these textural changes into an anomaly measure were formulated for early failure precursor observation and sensing. STSA was used to process the time series data from the constructed electronic circuit board experiment to estimate the extent of failure precursors, much earlier and with much less uncertainty than what was possible with the current state-of-the-art pattern recognition methods such as Principal Component Analysis and Neural Networks. This is due to the fact that unlike other techniques, STSA exploits the slow non-stationary dynamics of anomaly compared to the rest of the system dynamics. As the anomaly grows slowly, there is a small change in the pattern followed by the state variables under stationary conditions. After a while, a small change in anomaly could result in a sudden change in the pattern (phase plot) followed by the state variables. This sudden change is analogous to a failure and it is easily detected by many data processing techniques. The small change in the pattern that precedes the sudden change is the failure precursor which is not easily detected by PCA or neural networks. We have successfully implemented STSA on a circuit board experiment to detect this precursor.

The advantages of our novel STSA approach for PHM and anomaly detection are summarised below:

- capability of very early prognosis of failures in electrical systems
- real-time execution of the failure precursor sensing algorithm on inexpensive general-purpose microcomputers
- robustness of the algorithm resulting from its dependence on coarse graining of the time series data, instead of heavily relying on large order differential equations
- compatibility with commercial-of-the-shelf equipment with available signals without any additional sensors
- proof of concept with highly repeatable experimental validation on non-linear hybrid electronic circuit boards.

The Symbolic Time Series based methodology is briefly described here. Relevant system outputs are sampled at a suitable rate to obtain time series data. The time series is then transformed into wavelet coefficients. The wavelet coefficients are converted to symbols by partitioning. The partition is obtained with one particular data set chosen as nominal. The partition remains invariant in the subsequent analysis. As the dynamical behaviour of the system changes due to anomalies, symbol sequences generated are expected to change as well. Probabilistic Finite State Automata (Vidal et al., 2005) are used to model the dynamics of the symbol sequences. A special class of PFSA called the D-Markov Machine (Ray, 2004) is utilised for representing symbol sequences. The probability distributions, obtained from D-Markov Machines, provide a statistical representation to the symbol sequences. The variations in symbol patterns are quantified by the divergence among the probability distributions. A salient feature of this approach is that symbols are generated from wavelet coefficients instead of time series data. The advantages of using wavelet coefficients for symbol generation are provided in Rajagopalan and Ray (2006).

This paper is organised into six sections including the current one. Section 3 describes wavelet based pre-processing of time series data. The various aspects of Symbolic Dynamics analysis such as symbol generation, D-Markov machine construction are described in Section 3. Section 4 presents the STSA based anomaly detection methodology. Section 5 describes the experimental apparatus and provides the anomaly detection results on a non-linear system described by the Van der Pol equation (Khalil, 1996). Section 7 summarises and concludes the paper with recommendations for future work.

## 2 Preprocessing with wavelets

Preprocessing of time series data is often necessary for extraction of pertinent information. Fourier analysis is sufficient if the signal to be analysed is stationary and if the time period is accurately known. However, Fourier analysis may not be appropriate if the signal has non-stationary characteristics such as drifts and frequency trends. To mitigate this problem, small sections of the signal are analysed at various time instants. This technique is known as Short-Time Fourier Transform (STFT). It maps a signal into a two dimensional function of time and frequency. The STFT represents a sort of compromise between time and frequency-based views of a signal and it provides some information about both. However, the information can be obtained with limited precision, and that precision is determined by the size of window. Fixed size of window is the main drawback of STFT.

The wavelet transform was introduced to overcome the difficulties mentioned before. Wavelet analysis alleviates these difficulties via adaptive usage of long windows for

retrieving low frequency information and short windows for high frequency information (Mallat, 1998). The ability to perform flexible localised analysis is one of the striking features of wavelet transform. In addition to this, wavelet preprocessing helps in noise mitigation. Wavelet preprocessing for STSA consists of two steps namely:

- selection of appropriate wavelet basis
- selection of scales and obtaining the wavelet coefficients for the chosen scales.

Choice of wavelet primarily depends on the signal that is being analysed. In this paper, Daubechies wavelets (Mallat, 1998) are utilised for pre-processing. Daubechies wavelets provide the compactly supported wavelets with extremal phase and highest number of vanishing moments for a given support width. The last property is particularly beneficial since, in nonlinear systems, anomalies may manifest as higher order harmonics in system outputs.

For every wavelet, there exists a certain frequency called the centre frequency  $F_c$  that has the maximum modulus in the Fourier transform of the wavelet. The pseudo-frequency  $f_p$  (Abry, 1997; Wavelet Toolbox, 2006) of the wavelet at a particular scale  $\alpha$  is given in terms of the centre frequency  $F_c$  and the sampling interval  $\Delta t$  as

$$f_p = \frac{F_c}{\alpha \Delta t}. \quad (1)$$

The Power Spectral Density (PSD) of the signal provides the information about the frequency content of the signal. This information along with equation (1) can be used for scale selection. The procedure of selecting the scales is summarised below:

Perform PSD analysis on the time series data to find the frequencies of interest.

Substitute the above frequencies in place  $f_p$  of in equation (1) to obtain the respective scale  $\alpha$  in terms of the known parameters  $F_c$  and  $\Delta t$ .

The wavelet coefficients of the signal are significantly large when the pseudo-frequency  $f_p$  of the wavelet corresponds to the locally dominant frequencies in the underlying signal. Upon selection of the wavelet basis and scales, the wavelet coefficients are obtained at the chosen scales. These coefficients are stacked at selected time-shift positions, starting with the smallest scale and ending with the largest scale and then back from the largest value to the smallest value of the scale at the next instant of time shift. In the sequel, this one-dimensional array of arranged wavelet coefficients is called the scale series data. For symbol generation, the scale series data is handled in a similar way as time series data (Ray, 2004). The next section provides a brief review of symbolic dynamics.

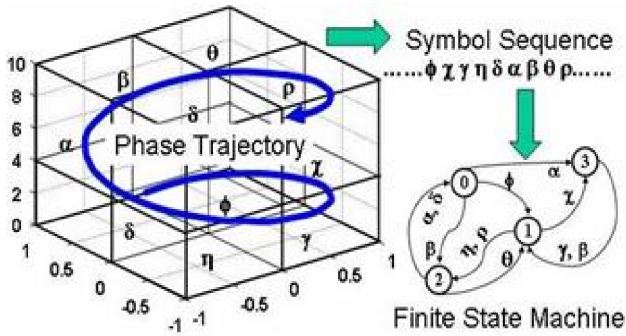
### 3 Review of Symbolic Time Series Analysis (STSA)

Continuously varying physical processes are often modelled as a finite-dimensional dynamical system:

$$\frac{dx}{dt} = f(x(t), \theta); \quad x(0) = x_0 \quad (2)$$

where  $t \in [0, \infty]$  is time;  $x \in R^m$  is the state vector in the phase space; and  $\theta \in R^n$  is the (slowly varying) parameter vector. Formally, a solution to equation (2) can be expressed as a continuous function of the initial state  $x_0$  as  $x(t) = \Phi_t x_0$ , where  $\Phi_t$  represents a parametric family of maps of the phase space into itself. This evolution of phase trajectory in (discrete) time  $t$  can be viewed as a flow of points in the phase space. A symbolic description is derived by partitioning the phase space into mutually disjoint regions as illustrated in Figure 1. A brief discussion on partitioning follows.

**Figure 1** Continuous dynamics to symbolic dynamics



A compact (i.e., closed and bounded) region  $\Omega$  within which the stationary part of the phase trajectories are contained is identified. Encoding of  $\Omega$  is accomplished by introducing a partition  $\mathcal{B} \equiv \{B_0, \dots, B_{m-1}\}$  consisting of  $m$  mutually exclusive and exhaustive cells. The dynamical system describes an orbit  $\sigma \equiv \{x_0, x_1, \dots, x_n, \dots\}$  in  $\Omega$ , which passes through or touches the cells of the partition  $\mathcal{B}$ . Each cell is labeled by a symbol  $s \in \mathcal{A}$ . The set  $\mathcal{A}$  of  $m$  distinct symbols that label the partition elements is called the *symbol alphabet*.

In general, every initial state  $x_0 \in \Omega$  generates a unique sequence of symbols defined by a mapping from the phase space to the symbol space:  $x_0 \mapsto s_{i0} s_{i1} s_{i2} \dots s_{i1} \dots$ . This mapping is called *Symbolic Dynamics* (Lind and Marcus, 1995) as it attributes a legal symbol sequence to the system dynamics starting from an initial state. Since the size of each cell is finite and also the cardinality of the alphabet is finite, any such symbol sequence represents, through iteration, a phase trajectory that has the compact support  $\Omega$ . In general, a dynamical system would only generate a subset of all possible sequences of symbols as there could be some illegal (i.e., physically inadmissible) sequences.

Symbolic dynamics can be viewed as coarse graining of the phase space, which is subjected to (possible) loss of information resulting from measurement imprecision and sensitivity to initial conditions. However, the essential robust features (e.g., periodic behaviour or chaotic behaviour of an orbit) are expected to be preserved in the symbol sequences through an appropriate partitioning of the phase space.

#### 3.1 Symbol generation

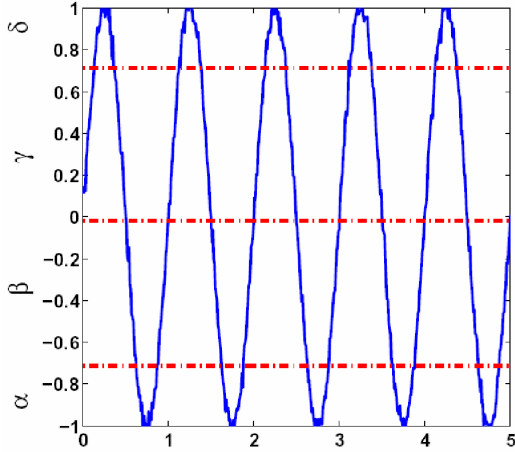
Various methods have been suggested in literature for symbolisation. These include variance-based (Veenman et al., 2002) and entropy-based (Chau and Wong, 1999) methods as well as hierarchical clustering. A survey of various clustering techniques is provided in Warren Liao (2005). In addition to these methods, another scheme of partitioning, based on symbolic false nearest neighbours (SFNN), was introduced in Kennel and Buhl (2003). The objective of SFNN partitioning is to ensure that points that are close to each other in symbol space are also close to each other in phase space. Partitions that yield a smaller proportion of symbolic false nearest neighbours are considered optimal. However, this partitioning method may become computationally very inefficient if the dimension of the phase space is large or if the data set is contaminated by noise, since noise induces false symbols.

In this paper, an entropy based partitioning scheme (Rajagopalan and Ray, 2006) is employed to generate the symbols. A partition that maximises the entropy of the generated symbol sequence is chosen as the candidate partition. In other words, this partition induces a uniform distribution of symbols for the nominal pattern. This method of maximum entropy partitioning is abbreviated as *ME* partitioning in the sequel. The procedure for obtaining a *ME* partition, for one dimensional data, is described below.

Let  $N$  be the length of the data set and  $|A|$  be the size of the alphabet (i.e., the number of the disjoint elements in the partition). The data is sorted in ascending order. Starting from the first point in the sorted data, every consecutive data segment of length  $\lfloor N/|A| \rfloor$  forms a distinct element of the partition. (Note:  $\lfloor x \rfloor$  represents the greatest integer less than or equal to  $x$ .)

With *ME* partitioning, information-rich regions are allocated more symbols and hence a finer partition is achieved in such regions. Similarly, regions with sparse information content are allocated fewer symbols leading to a coarser partition in those regions. Hence, even small variations in patterns are more likely to be detected in the symbol sequence obtained under *ME* partitioning than other partitioning. Figure 2 shows a *ME* partitioning for the noise contaminated signal  $\sin(2\pi t)$  with  $|A| = 4$ . As expected, the sizes of the partitions are not equal, but the probabilities of the symbols are equal.

**Figure 2** Maximum entropy partitioning with  $|A| = 4$



### 3.2 Pattern representation with D-Markov machine

This section describes the D-Markov machine for modelling symbol sequences. The core assumption here is a stochastic symbolic process can be approximated to a desired level of accuracy as a  $D$ th order Markov chain where  $D \in \mathcal{N}$ , the set of positive numbers.

**Definition 1:** A stochastic symbolic process  $S$  is called  $D$ th order Markov process if the probability of the current observation depends only on the previous  $D$  observations, i.e.,  $\forall k, \forall s_k \in A$

$$P[s_k / s_{k-1}s_{k-2} \dots s_0] = P[s_k / s_{k-1}s_{k-2} \dots s_{k-D}]. \quad (3)$$

In other words, the process has a memory of length  $D$ . Such a process can be represented as a Probabilistic Finite State Automaton. The states of the automaton are represented by symbol strings of length  $D$ , defined over the alphabet  $A$ . For example, with an alphabet  $A = \{0, 1\}$  and depth  $D = 2$ , the possible states are  $\{00, 01, 10, 11\}$ . The machine transitions from one state to another upon occurrence of a symbol  $s_k \in A$ . Figure 3 depicts a D-Markov Machine with  $|A| = 2$  and  $D = 2$ .

The D-Markov machine can be represented by its state transition matrix  $\Pi$  or by its state probability vector  $p$ . The  $\Pi$  matrix is a stochastic matrix, i.e., all row sums are equal to one. The elements of the  $\Pi$  matrix represent the probabilities of transition from one state to another. For example,  $\pi_{23}$  represents the probability of transition from state 2 to state 3. The state transition probabilities of a D-Markov can be experimentally determined from the symbol sequence by frequency counting. The elements of state probability vector  $p$  represent the probability of states of the D-Markov Machine.

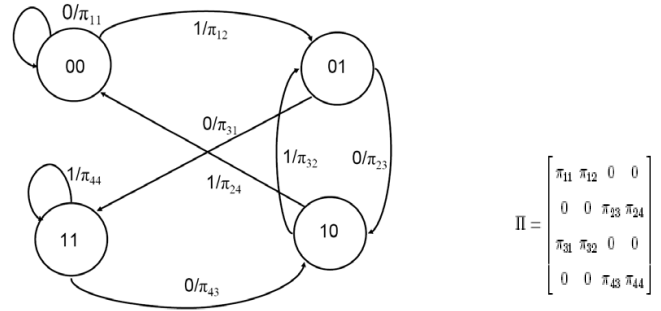
The construction of a D-Markov machine is fairly straightforward. For a specific  $D \in \mathcal{N}$ , the states are defined as above. On a given symbol sequence, a moving window of length  $(D + 1)$  is used to count the occurrence of finite symbol strings  $s_{i1}s_{i2} \dots s_{iD}s_{i(D+1)}$  and  $s_{i1}s_{i2} \dots s_{iD}$ , which are respectively denoted by  $N(s_{i1}s_{i2} \dots s_{iD}s_{i(D+1)})$  and  $N(s_{i1}s_{i2} \dots s_{iD})$ . Note that if  $N(s_{i1}s_{i2} \dots s_{iD}) = 0$ , then the state

$s_{i1}s_{i2} \dots s_{iD} \in Q$  has zero probability of occurrence. For  $N(s_{i1}s_{i2} \dots s_{iD}) \neq 0$ , the transition probabilities are then obtained by these frequency counts as follows:

$$\pi_{jk} = \frac{P(s_{i1}s_{i2} \dots s_{iD}s)}{P(s_{i1}s_{i2} \dots s_{iD})} \approx \frac{N(s_{i1}s_{i2} \dots s_{iD}s)}{N(s_{i1}s_{i2} \dots s_{iD})}$$

where, the corresponding states are denoted as:  $q_j \equiv s_{i1}s_{i2} \dots s_{iD}$  and  $q_k \equiv s_{i2} \dots s_{iD}s$ . The total number of states in a D-Markov machine is less than or equal to  $|A|^D$  since some of the states might be forbidden, implying that the probabilities of these states are zero.

**Figure 3** D-Markov machine and  $\Pi$  matrix



The depth of the D-Markov machine is a crucial parameter since the number of states varies exponentially with  $D$ . A very small depth could mean insufficient memory for the D-Markov machine to appropriately represent the symbolic dynamics of the process. On the other hand, an unnecessarily large  $D$  would result in a large number of states, leading to extremely small values of state probabilities and an inaccurate  $\Pi$  matrix. A procedure based on entropy rate has been developed for selecting the depth of the D-Markov machine. The key idea is that increasing the depth beyond a certain value does not lead to any appreciable change in entropy; equivalently, the entropy rate would be very small.

**Definition 2:** Given the current state, the entropy rate,  $h_\mu$ , of a symbolic stochastic process is defined as the uncertainty in the next symbol

$$h_\mu = -\sum_{i=1}^L p_i \sum_{j=1}^{|A|} \tilde{\pi}_{ij} \log_2 \tilde{\pi}_{ij}. \quad (4)$$

where  $p_i$  is the probability of occurrence of  $i$ th state,  $\tilde{\pi}_{ij}$  is the probability of occurrence of  $j$ th symbol in the  $i$ th state;  $L$  is the number of states in the probabilistic finite state machine and  $|A|$  is the alphabet size.

Being a measure of uncertainty, the entropy rate  $h_\mu$  monotonically decreases as the depth  $D$  of the D-Markov machine is increased. Beyond a certain point, increasing  $D$  may not lead to any appreciable change in the entropy rate. This is the asymptotical entropy rate and the corresponding  $D$  is optimal for the machine. With ideal noise-free data  $h_\mu$  converges to zero. However, with real world noisy data,  $h_\mu$  may only monotonically decrease to a small non-zero

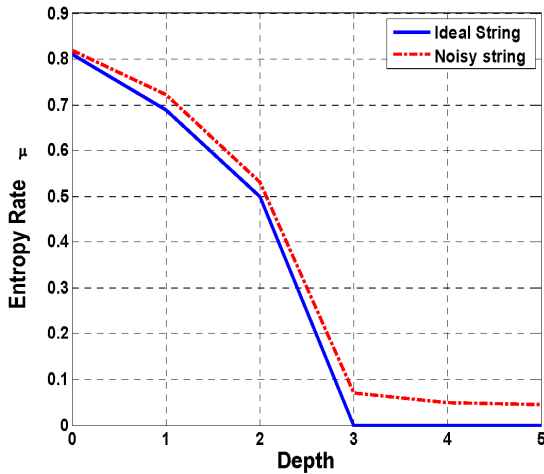
value, depending on the magnitude and the type of noise. Thus, the test for the optimum  $D$  relies on how  $h_\mu$  converges as  $D$  is increased.

For example, let us consider a data set that yields a symbol stream  $S = \{000100010001 \dots\}$  on the alphabet  $A = \{0, 1\}$ . Table 1 provides the entropy rate of the inferred D-Markov machine for various depths. It can be seen that the number of states in the generated machine remains the same for depth  $D \geq 3$ . Correspondingly, the entropy rate remains at zero. This implies the optimum depth for correct representation for this symbol stream is three. The curve, shown in Figure 4 by solid lines, exhibits the plot of  $h^1$  of the inferred machine as  $D$  is increased.

**Table 1** Entropy rate values

Depth	Entropy rate for ideal data	Entropy rate for noisy data
0	0.810	0.818
1	0.689	0.721
2	0.500	0.530
3	0.000	0.070
4	0.000	0.050
5	0.000	0.045

**Figure 4** Entropy rate vs. depth



Next, let us consider the case where a small amount of white noise is added to the raw data that produced the symbol stream  $S$ . From Table 1, it can be observed that the change in entropy rate is very small beyond  $D = 3$ . This means that very little information is gained by increasing the depth and the uncertainty in the system is largely due to the noise. Hence a criterion for the selection of optimal depth of the D-Markov machine can be established in terms of a lower bound on the change in the entropy rate. The curve, shown in Figure 4 by dashed lines, exhibits the plot of  $h_\mu$  of the inferred machine as  $D$  is increased.

### 3.3 Anomaly measures

The D-Markov machine, described above, is capable of representing patterns observed in the symbol sequences.

In order to quantify the similarity or diversity in the patterns, a measure needs to be defined. This measure is called an anomaly measure  $M$  since it measures the deviations of anomalous patterns from the nominal pattern. The induced norm of the difference between the nominal state transition matrix  $\Pi_0$  and the state transition matrix for the current pattern  $\Pi_k$  is a viable candidate for the anomaly measure, i.e.,

$$M_k = \|\Pi_0 - \Pi_k\|. \quad (5)$$

Alternatively, measures of anomaly may be derived directly from the state probability vector  $p$  of the D-Markov machine, which is the left eigenvector corresponding to the unique unity eigen value of the (irreducible) matrix. A measure can be defined as:

$$M_k = \|p_0 - p_k\|. \quad (6)$$

Another candidate for the anomaly measure is the angle between the state probability vectors

$$M_k = \arccos\left(\frac{\langle p_0, p_k \rangle}{\|p_0\| \|p_k\|}\right). \quad (7)$$

## 4 STSA based anomaly detection and calibration procedure

Having discussed various tools and techniques of Symbolic Dynamics, this section outlines the steps of the *forward problem* and the *inverse problem* in the STSA approach introduced in earlier section. The solution of the forward problem allows calibration of the anomaly measure against the actual value of an anomalous parameter. Following are the steps for the *forward problem*:

- F1 Selection of an appropriate set of input stimuli and generation of time series data with chosen input
- F2 Preprocessing of time series with appropriate wavelet basis
- F3 Generate symbol sequences through partitioning
- F4 State machine construction from symbol sequences and determination of the connection matrix
- F5 Selection of an appropriate anomaly measure  $\mathbf{M}$
- F6 Formulation and calibration of a (possibly non-parametric) relation between the computed anomaly measure and known physical anomaly at different (slow-time) epochs.

The solution of the *inverse problem* along with the forward problem solution allows estimation of the anomalous parameter value. Following are the steps for the *inverse problem*:

- I1 Excitation with known input stimuli selected in the forward problem and generation of the stationary behaviour as time series data

- 12 Preprocessing with wavelet chosen in *forward problem*
- 13 Generating symbol sequences with partitioning determined in the *forward problem*
- 14 State Machine construction using the symbol sequence
- 15 Computing the anomaly measure **M**
- 16 Detection and identification of an anomaly, if any, based on the computed anomaly measure and the relation derived in Step F6 of the forward problem.

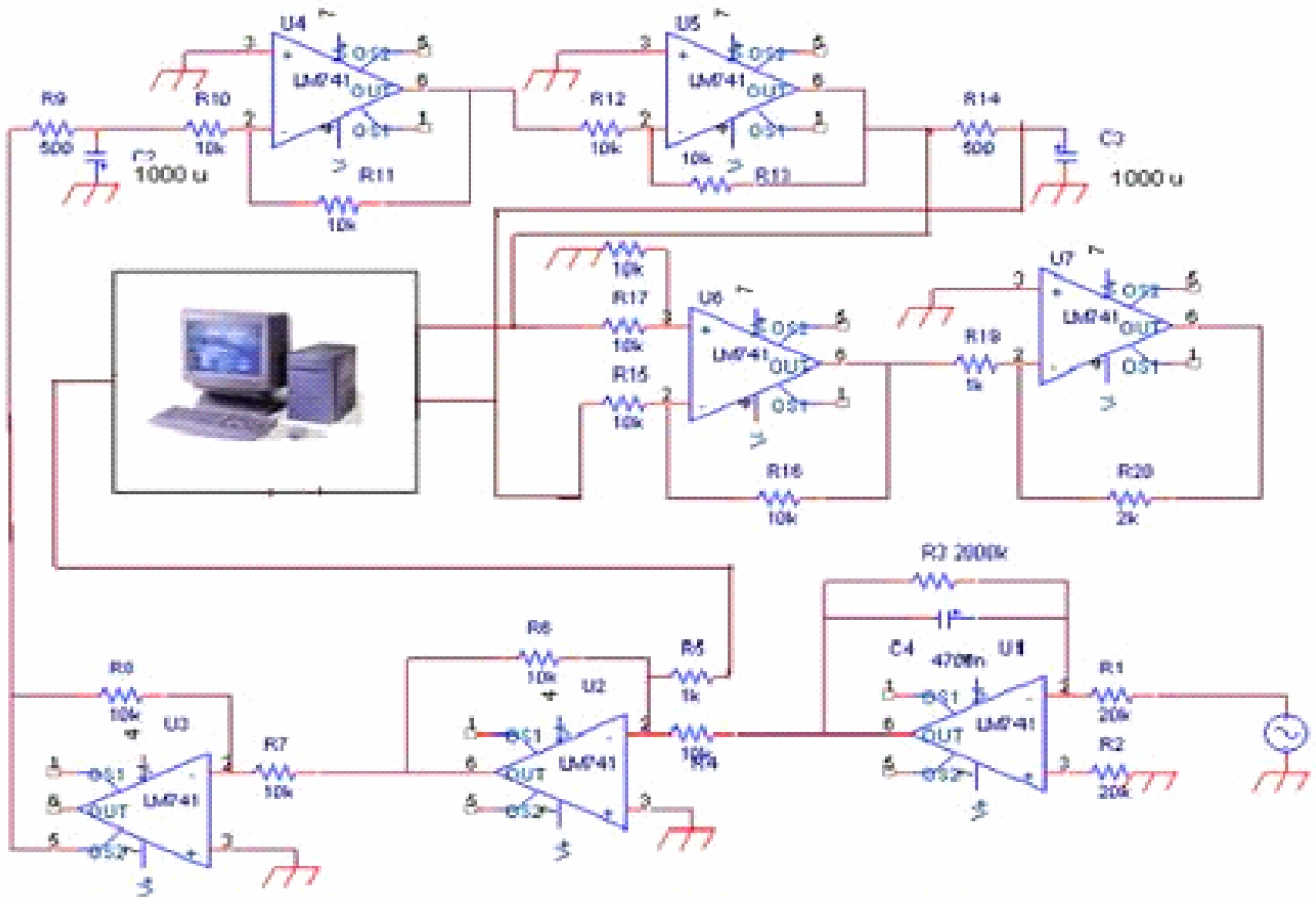
**5 Experimental results**

This section provides a description of the experimental apparatus and discusses the results of anomaly detection in a non-linear system described by the Van der Pol equation.

*5.1 Description of experimental apparatus*

Figure 5 shows the implementation of a resistance-capacitor circuit that is coupled with the MATLAB-based real-time software through A/D and D/A channels. The non-linearity and other parameters that modify the linear circuit to that of the Van der Pol oscillator are generated in the software and the generated signal is fed back to the electronic circuit via D/A channel. The experimental setup consists of a computer with Keithley 1801HC data acquisition board with 64 A/D and 4 D/A channels; the experimental circuit board is connected to the data acquisition board. A 15 volt dual power supply is used to power the circuit board; An oscilloscope is utilised to monitor circuit board signals. It also consists of a mouse, keyboard and monitor to interactively input anomalous parameter and monitor the predictions for the anomalous parameter. A signal generator is used for injecting signals into the circuit board.

**Figure 5** Experimental apparatus



## 5.2 Van der Pol oscillator circuit board

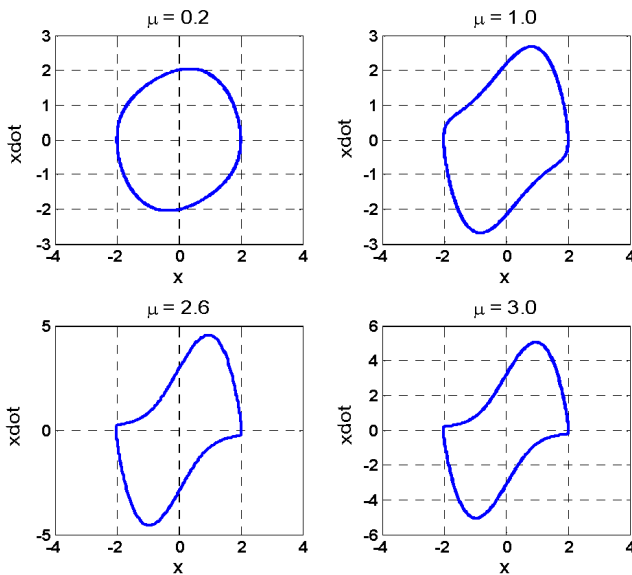
This section presents the results of anomaly detection experimentation on the electronic circuit apparatus, whose dynamics are governed by the Van der Pol equation (Khalil, 1996) as follows.

$$\frac{d^2 x}{dt^2} - \mu(1-x^2) \frac{dx}{dt} + x = 0. \quad (8)$$

The parameter  $\mu$  varies slowly with time. The nominal value of  $\mu$  is 0.2 and the variations in  $\mu$  are treated as anomalies. Figure 6 shows the phase plots of the systems for four different values of  $\mu$ . For a small value ( $\mu = 0.2$ ), the phase plot is a fairly smooth orbit that is close to a circle of radius 2. For a medium value ( $\mu = 1.0$ ), the shape of the orbit is distorted as seen in Figure 6. For large values ( $\mu > 2.5$ ), the closed orbit is severely distorted. As stated earlier, the objective is to detect the variations in  $\mu$  as early as possible, before they manifest as severe distortions in the phase behaviour.

As evident from the phase plots in Figure 5, the range of the signal  $x(t)$  is almost unaffected by the variations in  $\mu$ , whereas that of the signal  $dx/dt$  is significantly increases as  $\mu$  increases; consequently, the phase-plots become significantly distorted for larger values of  $\mu$ . Hence, it would appropriate to utilise  $dx/dt$  for STSA.

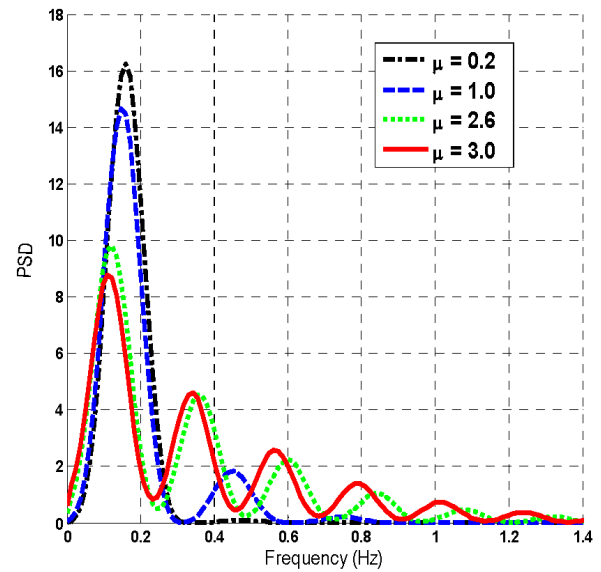
**Figure 6** Phase plots for different values of  $\mu$



The plots in Figure 7 depict the power spectrum profile for the values of  $\mu$  at 0.2, 1.0, 2.6 and 3.0. The power of the signal, in the nominal case (i.e., at  $\mu = 0.2$ ), is confined to a relatively narrow frequency band of 0.0–0.25 Hz while the power is gradually spread across a greater range in the anomalous cases as  $\mu$  increases. Hence, choosing frequencies that are present in the anomalous cases, but are absent in the nominal case ( $\mu = 0.2$ ), would aid in anomaly detection. In this case, we chose frequencies in the range of 0.7–1.0 Hz. The power in this band is almost negligible in

the nominal case and even for small variations in  $\mu$  ( $< 1.0$ ). As the anomaly progresses, the power is increasingly dispersed in the afore-mentioned range. Hence, if scales are chosen corresponding to these frequencies, then the ranges of wavelet coefficients under anomalous conditions would be far greater in magnitude than those at the nominal or nearly nominal conditions. Thus, gradually evolving anomalies can be detected at an early stage, because symbols generated from such coefficients would differ from each other. The signal  $dx/dt$  exhibits sharp peaks as the anomaly progresses. Hence, it would be appropriate to choose a wavelet that also exhibits sharp peaks in its profile. With this consideration in mind, wavelet ‘db20’ was chosen as the mother wavelet.

**Figure 7** Power spectrum plots



Wavelets coefficients are generated with wavelet ‘db20’. These coefficients are partitioned to generate symbols. Once the partitioning is created, it remains invariant. As the dynamical behaviour of the system changes due to variations in  $\mu$ , the statistical characteristics of the symbol sequences are also altered and so are the symbol probabilities.

## 5.3 Comparison of various analyses of the experimental data

This section compares the results of anomaly detection of three techniques:

- Symbolic Time Series Analysis (STSA)
- Principal Component Analysis (PCA)
- radial basis function neural network.

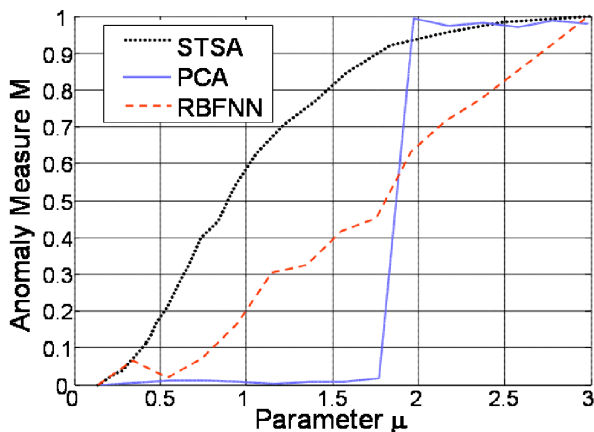
The details of PCA and Radial Basis Function Neural Network based anomaly detectors are provided in Chin et al. (2005). All anomaly measures are normalised to one for comparison purposes using the maximum value of the anomaly for the experimental range of  $\mu$ .

### 5.3.1 Principal Component Analysis (PCA)

The length of the dataset  $L = 4995$ . Upon trial and error, each dataset was divided into  $d = 333$  segments to obtain best possible results, each of length  $n = 15$ .  $d = L/n$  where  $N = 15$  and  $L = 4995$ . The  $d$  segments were arranged to form a data matrix of size  $333 \times 15$  ( $d \times n$ ). The resulting covariance matrix yields 15 eigen values of which only two are significant. The  $M$  matrix is constructed with the eigenvectors corresponding to these eigen values. The angle between  $M$  matrices at nominal and anomalous conditions is the anomaly measure.

Figure 8 shows that PCA detects the anomaly once the distortion is apparent in the phase behaviour, but fails to provide early detection. It is a yes/no type of anomaly detection. This may be due to the fact that PCA, being a linear feature extractor, may not be appropriate for a system that is inherently non-linear. PCA tries to impose a linear structure to the system. When the properties of the system have changed (for high values of  $\mu$ ), the linear structure imposed by the PCA is significantly different from the one at the nominal condition ( $\mu = 0.1$ ). At this stage, the anomaly measure increases abruptly. For further distortions, change in the linear structure is minimal and the anomaly measure remains more or less the same.

Figure 8 Anomaly measure plots



### 5.3.2 Radial Basis Function Neural Net (RBFNN)

The length of the dataset  $L = 5000$  and  $\alpha = 0.5$ .  $\alpha$  in the range  $[0.1, 0.7]$  also yielded similar results. It can be seen that anomaly measure based on RBFNN fluctuates initially and lacks the monotonic property. It can be seen in Figure 8 that anomaly measure increases monotonically with the anomaly after the initial fluctuations.

### 5.3.3 Symbolic Time Series Analysis (STSA)

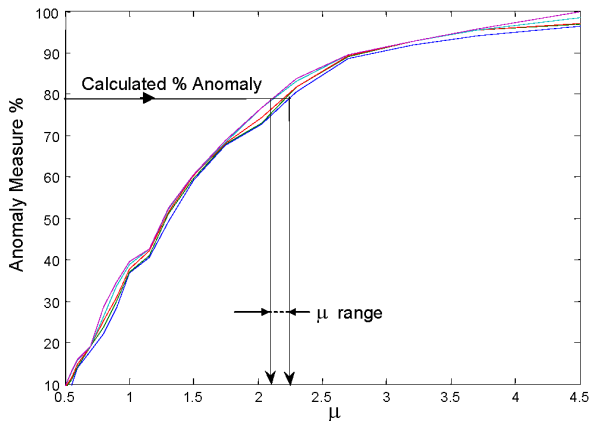
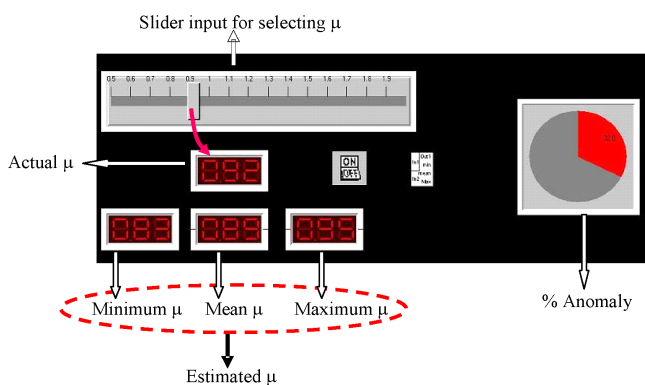
With the following parameter values, the STSA was found to work quite accurately and robustly compared to other techniques: Number of Symbols = 8, Depth = 1,

Wavelet = 'db20', Transform = Continuous Wavelet Transform and Wavelet coefficient partitioning scales = [95.2381 88.8889 83.3333 78.4314 74.0741 70.1754 66.6667].

In Figure 8, it can be seen that the anomaly measure is small for low values of  $\mu$  ( $< 1.0$ ). Once the distortion occurs (beyond  $\mu = 1.0$ ), the anomaly measure changes rapidly. This increase in the slope and curvature of the anomaly measure provides an opportunity for early detection. This, however, is difficult to achieve with RBFNN since the increase in the measure was linear. Thus symbolic dynamics has a significant advantage over RBFNN as far as early detection is concerned. At higher values of  $\mu > 2.4$ , the distortion of phase plot remains more or less the same. The anomaly measure reflects this with just a marginal increase in the above mentioned range. Thus anomaly measure obtained with symbolic dynamics adequately illustrates the state of the system for all values of  $\mu$  in the experimental range. The STSA based anomaly measure is monotonically increasing, smooth and shows a much earlier rise than RBFNN based technique. The RBFNN technique could be theoretically improved with perhaps better tuning parameters but that requires significant trial-and-error to achieve the tuning and there is no guaranteed procedure for success in this approach.

## 6 Inverse problem solution

The inverse problem (of predicting the anomaly given the time series data) was also solved. A series of experiments were conducted to calibrate the anomaly measure. Repeated experiments resulted in different time series data sets which were processed using STSA technique. The percent anomaly measure for five different experiments is shown in Figure 8. The repeatability and consistency of STSA technique in estimating anomaly is remarkable. It resulted in a narrow 'anomaly band'. Due to the monotonic nature of the plot, each value of anomaly can be associated with a continuous range of values of  $\mu$ . For convenience, a Graphical User Interface (GUI) was created (Figure 10). This GUI accepts a value of anomalous parameter  $\mu$  from the user as an input and displays the selected actual value of  $\mu$ . There is an on/off switch on the screen to turn on the anomaly detection. Upon turning on the anomaly detection, the system waits to reach a stationary signal behaviour and collects bursts of data. The data is passed through the STSA steps and an anomaly measure is calculated which is displayed by the pie chart as a percentage. Using this calculated anomaly measure and the chart in Figure 9, estimated values minimum  $\mu$ , mean  $\mu$ , and maximum  $\mu$  are displayed on the screen. Execution of the complete experiment for various selected values of  $\mu$ , resulted in accurate estimation of the range of  $\mu$  and a mean value estimation of  $\mu$  that was always within 7% of the actual selected  $\mu$  in the range 0.5–2.0.

**Figure 9** STSA repeatability permits inverse problem solving**Figure 10** GUI interface

## 7 Summary and conclusions

Experimental data was collected from the electronic circuit board and analysed using three techniques, *viz.*, STSA, PCA and neural networks. PCA did not result in a gradual anomaly detection technique. It resulted in yes/no type of anomaly prediction. This is reasonable due to linear nature of the technique and non-linear nature of the circuit. Neural networks approach took a lot of trial-error effort in coming up with a good neural network structure and training the neural network. The anomaly plots were gradual with slight fluctuations. The robustness of the technique was not the greatest compared to the symbolic dynamic technique. Identical experiments showed slightly fluctuating (decreasing anomaly measure with increasing anomaly) results. This lead to a thick band of anomaly plots using neural networks. Due to the thick band, the implementation of the inverse problem (prognostics) did not work accurately with neural networks.

Symbolic dynamic technique resulted in a monotonically increasing smooth anomaly plot which was experimentally repeatable to a remarkable accuracy as shown in Figure 9. For the Vander Pol oscillator circuit board experiment, this lead to consistently accurate predictions for the anomaly parameter  $\mu$  and its range.

## References

- Abry, P. (1997) *Ondelettes et Turbulence. Multiresolutions, Algorithmes de Decomposition, Invariance D'chelles*, Diderot Editeur, Paris.
- Chau, T. and Wong, A.K.C. (1999) 'Pattern discovery by residual analysis and recursive partitioning', *IEEE Transactions on Knowledge and Data Engineering*, Vol. 11, No. 6, pp.833–852.
- Chin, S.C., Ray, A. and Rajagopalan, V. (2005) 'Symbolic time series analysis for anomaly detection: a comparative evaluation', *Signal Processing*, Vol. 96, No. 9, pp.1859–1868.
- Cover, T.M. and Thomas, J.A. (1991) *Elements of Information Theory*, John Wiley, New York.
- Kennel, M.B. and Buhl, M. (2003) 'Estimating good discrete partitions from observed data: symbolic false nearest neighbors', *Review Letters*, Vol. 91, p.084102.
- Khalil, H.K. (1996) *Nonlinear Systems*, 2/e, Prentice-Hall Inc., Upper Saddle River, New Jersey, USA.
- Lind, D. and Marcus, M. (1995) *An Introduction to Symbolic Dynamics and Coding*, Cambridge University Press, UK.
- Mallat, S. (1998) *A Wavelet Tour of Signal Processing*, 2/e, Academic Press, San Diego, California, USA.
- Rajagopalan, V. and Ray, A. (2006) 'Symbolic time series analysis via wavelet-based partitioning', *Signal Processing*, Vol. 86, No. 11, pp.3309–3320.
- Ray, A. (2004) 'Symbolic dynamic analysis of complex systems for anomaly detection', *Signal Processing*, Vol. 84 No. 7, pp.1115–1130.
- Veenman, C.J., Reinders, M.J.T., Bolt, E.M. and Baker, E. (2002) 'A maximum variance cluster algorithm', *IEEE Transactions on Pattern Analysis and Machine Intelligence*, Vol. 24, No. 9, pp.1273–1280.
- Vidal, E., Tollard, F., Higuera, C., Casacuberta, F. and Carrasco, R.C. (2005) 'Probabilistic finite-state machines, part I', *IEEE Transactions on Pattern Analysis and Machine Intelligence*, Vol. 27, No. 7, pp.1013–1025.
- Warren Liao, T. (2005) 'Clustering of time series data – a survey', *Pattern Recognition*, Vol. 38, pp.1857–1874.
- Wavelet Toolbox (2006) *MATLAB*, Mathworks Inc., Natick, Massachusetts, USA.